

Symbolic Synchronization and the Detection of Global Properties of Coupled Dynamics from Local Information

Sarika Jalan,^{*} Jürgen Jost,[†] and Fatihcan M. Atay[‡]

Max Planck Institute for Mathematics in the Sciences, 04103 Leipzig, Germany

(Dated: May 3, 2018)

Abstract

We study coupled dynamics on networks using symbolic dynamics. The symbolic dynamics is defined by dividing the state space into a small number of regions (typically 2), and considering the relative frequencies of the transitions between those regions. It turns out that the global qualitative properties of the coupled dynamics can be classified into three different phases based on the synchronization of the variables and the homogeneity of the symbolic dynamics. Of particular interest is the *homogeneous unsynchronized phase* where the coupled dynamics is in a chaotic unsynchronized state, but exhibits (almost) identical symbolic dynamics at all the nodes in the network. We refer to this dynamical behaviour as *symbolic synchronization*. In this phase, the local symbolic dynamics of any arbitrarily selected node reflects global properties of the coupled dynamics, such as qualitative behaviour of the largest Lyapunov exponent and phase synchronization. This phase depends mainly on the network architecture, and only to a smaller extent on the local chaotic dynamical function. We present results for two model dynamics, iterations of the one-dimensional logistic map and the two-dimensional Hénon map, as local dynamical function.

^{*}Electronic address: sjalan@mis.mpg.de

[†]Electronic address: jjost@mis.mpg.de

[‡]Electronic address: atay@member.ams.org

Nonlinear dynamical elements interacting with each other can lead to synchronization or other types of coherent behaviour at the system scale. Coupled map models are one of the most widely accepted models to understand these behaviours in systems from many diverse fields such as physics, biology, ecology etc. Their important feature is that the individual elements can already exhibit some complex behaviour, for example chaotic dynamics. The question then is how to detect coordination at larger scales beyond the simplest one, synchronization. An important tool in the analysis of dynamical systems are symbolic dynamics. We develop a new scheme of symbolic dynamics that is based on the special partitions of the phase space which prevent the occurrence of certain symbol sequences related to the characteristics of the dynamics. In particular, we report a new behaviour of coupled dynamics, which we refer to as symbolic synchronization, i.e. synchronization of the nodes at the coarse grained level, whereas microscopically all elements behave differently. Through the framework of this symbolic dynamics, we detect various global properties of coupled dynamics on networks by using a scalar time series of any randomly selected node. A decisive advantage of our method is that the global properties are inferred by using a short time series, hence the method is computationally fast, does not depend on the size of the network, and is reasonably robust against external noise.

I. INTRODUCTION

In order to gain insights into the behaviour of real systems from many diverse fields ranging from chemical, physical and biological systems, it is useful to identify model systems that on the one hand exhibit essential dynamical features of those real world systems, but on the other hand suppress individual details that are not really relevant for the qualitative behaviour [1]. Coupled map models have emerged as one such paradigm [2, 3]. Here, we have a system of elements with identical local dynamical functions. These elements are arranged in a network that expresses their couplings so that the local dynamical iteration depends not only on the own state of an element, but also on the ones of its neighbour in the network. The inhomogeneities in the network then translate into qualitative features of the global

dynamics. While such coupled map models already present an important simplification in view of the complexities of real world dynamics, their behaviour can nevertheless be sufficiently complicated and difficult to analyze. Thus, it is important to identify parameters that allow for a facile and robust detection of different qualitative states. One needs a coarse grained description to analyze the complicated time evolution of a chaotic dynamical system [4, 5]. In doing so one inevitably simplifies the dynamics a lot and some of the information are lost, but the aim is that important invariants and robust properties of the dynamical systems can be kept. Such a coarse graining means that we divide the possible dynamical states of the system into finitely many discrete classes and investigate the derived *symbolic dynamics* [4].

Coarse graining of the time evolution of lower dimensional systems have been studied at various levels [5, 6], but symbolic dynamical studies of higher dimensional spatio-temporal chaotic systems are rare and so far limited to coupled map lattices [7]. In the present paper, continuing the approach developed in [8], we study symbolic dynamics of coupled map networks and demonstrate that they can serve the above purpose well. Thereby, we attempt to provide a general framework for coupled dynamics on networks.

In [8], we have studied symbolic dynamics of a discrete dynamical iteration of a function based on non-generating partitions. We have shown two important uses of this symbolic dynamics, namely, distinguishing a chaotic iteration and a random iteration with the same density distribution (this is related to the earlier work on transition entropy [9] and [10] on permutation entropy), and detecting synchronization in coupled dynamics on large networks. In this paper we extend these studies and propose a general method to investigate collective behaviour of coupled systems. Besides the applications mentioned in [8], we show further applications of symbolic dynamics for detecting various dynamical properties of coupled dynamics in relation to structural parameters of the underlying network.

We take coupled map network models as generic models to apply our method. Chaotic coupled maps show rich spatio-temporal behaviour. One phenomenon that has received a lot of attention is synchronization, where different random or chaotic units of a system behave in unison [11, 12]. (For a selection of recent references, see also [13].) One application of our symbolic dynamics is the detection of synchronization in large complex systems. Traditional methods for the detection of synchronization in coupled systems focus on the correlation analysis of the time series measured at pairs of the nodes. In [8] we have introduced a

method based on symbolic dynamics, which uses a short time series of any single arbitrarily selected node to detect global synchrony of all the units. In this paper we show that the same type of symbolic dynamics can be used as a measure of phase synchronization, a phenomenon shown by coupled dynamics on networks [14].

In more detail, by our method we classify the coupled dynamics into different states, depending upon the synchronization of the nodes and the *homogeneity of the symbolic dynamics* of the nodes. The most interesting phase is the unsynchronized homogeneous phase, which refers to the state where the local chaotic dynamics of the individual nodes are different, but the derived symbolic dynamics of all the nodes are similar. We refer to this state as *symbolic synchronization* of the nodes. Recently, the unsynchronized region of coupled maps has been shown to have a fractal stationary density function [15]. We show that, in this phase, the transition probabilities of any randomly selected node reflect the qualitative information of the largest Lyapunov exponent (λ_l) and the phase synchronization of the coupled dynamics. For the calculation of the largest Lyapunov exponent we utilize only a short time series, whereas traditional methods to calculate the largest Lyapunov exponent from a scalar time series require rather long time series and also involve various computational complications [16]. We point out, however, that – as to be expected from such a simplistic reduction – our symbolic dynamics gives only the qualitative behaviour of the Lyapunov exponent λ_l , but of course not its exact value.

The paper is organized as follows. After an introductory section we introduce the definitions of the different phases based on the symbolic dynamical properties in Section II. In Section III, we then present numerical examples illustrating the behaviour of nodes in different phases. Mostly we present results for homogeneous synchronized phase which is of main interest. The key point is that the derived symbolic dynamics allows for the detection of the global properties of coupled dynamics from local measurements, that is, we can infer global properties of the dynamical network by considering the symbolic dynamics at a single node. Section IV distinguishes different dynamical phases based on the network parameters. Section V describes the relation between symbolic dynamics and phase synchronization. Section VI discusses the coupled Hénon map.

II. MODEL AND DEFINITION OF SYMBOLIC DYNAMICS

We consider the dynamical system defined by the iteration rule

$$x(t+1) = f(x(t)) \tag{1}$$

where $t \in \mathbb{Z}$ is the discrete time and $f : S \rightarrow S$ is a map on a subset S of \mathbb{R}^n . Let $\{S_i : i = 1, \dots, m\}$ be a partition of S , i.e., a collection of mutually disjoint and nonempty subsets satisfying $\cup_{i=1}^m S_i = S$. The symbolic dynamics corresponding to (1) is the sequence of symbols $\{\dots, s_{t-1}, s_t, s_{t+1}, \dots\}$ where $s_t = i$ if $x(t) \in S_i$. For the purposes of this paper, a useful partition is defined as follows. Let $x = (x_1, \dots, x_n) \in \mathbb{R}^n$, and suppose the scalar $x_{n'}$, $1 \leq n' \leq n$, is available for measurement. For a given threshold value $x^* \in \mathbb{R}$, define the sets

$$\begin{aligned} S_1 &= \{x \in S : x_{n'} < x^*\} \\ S_2 &= \{x \in S : x_{n'} \geq x^*\} \end{aligned} \tag{2}$$

The value $x_{n'}$ can be chosen to make the sets S_1, S_2 nonempty, in which case they form a non-trivial partition of S . For this special partition, we use the two-symbol dynamics generated by

$$s_t = \begin{cases} \alpha & \text{if } x'_{n'}(t) < x^* \\ \beta & \text{if } x'_{n'}(t) \geq x^*. \end{cases} \tag{3}$$

The symbolic dynamics depends only on the measurements $x_{n'}$, yielding a sequence of symbols determined by whether a measured value exceeds the threshold x^* or not. Essentially any choice of the threshold x^* will yield a non-generating partition. For practical calculations using short time series, however, a judicious choice of x^* becomes important. We will address this issue later in the paper (see section V).

We take the well known coupled map model [17],

$$x_i(t+1) = f(x_i(t)) + \frac{\varepsilon}{k_i} \sum_j w_{ij} g(x_j(t), x_i(t)) \tag{4}$$

where $x_i(t)$ is the dynamical variable of the i -th node ($1 \leq i \leq N$) at time t , w is the adjacency matrix with elements w_{ij} taking values between 0 and 1 depending upon the weight of the connection between i and j , and k_i is some normalization factor depending on the node i , for example its degree. The function $f(x)$ defines the local nonlinear map and the function $g(x)$ defines the nature of the coupling between the nodes. In the first three sections,

we present the results for the local dynamics given by the logistic map $f(x) = \mu x(1 - x)$ and coupling function $g(x_j(t), x_i(t)) = f(x_j(t)) - f(x_i(t))$. We take $\mu = 4$, for which logistic map exhibits chaotic behaviour with Lyapunov exponent $\ln(2)$. The weight w_{ij} is simply one when nodes i and j are neighbours in the undirected network, and 0 otherwise. In particular, the matrix w is symmetric; k_i then is the degree of node i , as already indicated.

We evolve Equation (4) starting from random initial conditions and estimate the transition probabilities using time series of length $\tau = 1000$. Note that the length of the time series is independent of the size of the network. We calculate the transition probability $P(i, j)$ by the ratio $\sum_t n(s_t = i, s_{t+1} = j) / \sum_t n(s_t = i)$, where n is a count of the number of times of occurrence [8].

III. DIFFERENT STATES OF THE COUPLED DYNAMICS

We classify the coupled dynamics in three different categories based on the dynamical behaviour, and we show that how one category differs from another based on some of the parameters of underlying network:

1. Unsynchronized or phase synchronized *non-homogeneous* behaviour : *phase one*,
2. Partially synchronized or phase synchronized *homogeneous behaviour* : *phase two*, and
3. Fully synchronized *homogeneous behaviour* : *phase three*.

Here, synchronization refers to the variables at different nodes having the same value $x_i(t) = x_j(t)$ for all i, j . The network is globally synchronized when at each time t , all nodes have the same value. Partial synchronization means that some of the nodes form a cluster inside which all the nodes are synchronized while they are not synchronized with the nodes in the different clusters. We note, however, that this state usually does not occur in our coupled dynamics because the phase differences between the various clusters will interfere with the internal synchronizations. The following behaviour, however, does robustly occur in suitable parameter regions. A pair of nodes is called phase synchronized [14] when they have their minima (maxima) matching for all $t > t_0$, that is, when one of them attains a minimum then so does the other. The concrete values may and can be different. In a phase synchronized cluster all nodes are phase synchronized.

Complete synchronization is indicated by the variance σ^2 of the variables over the network tending to zero, where

$$\sigma^2 = \left\langle \frac{1}{N-1} \sum_i [x_i(t) - \bar{x}(t)]^2 \right\rangle_t,$$

$\bar{x}(t) = \frac{1}{N} \sum_i x_i(t)$ denotes an average over the nodes of the network, and $\langle \dots \rangle_t$ denotes an average over time. We define *homogeneous* and *non-homogeneous* behaviour based on the symbolic dynamics of the individual nodes. If all the nodes have the same transition probabilities, then we say that the coupled dynamics is homogeneous; otherwise it is non-homogeneous. Homogeneity is indicated by the variance of the transition probability over the network being zero,

$$\varsigma^2 = \left\langle \frac{1}{N-1} \sum_{k=1}^N [P_k(\alpha, \alpha) - \overline{P(\alpha, \alpha)}]^2 \right\rangle \quad (5)$$

where $\overline{P(\alpha, \alpha)} = \sum_{k=1}^N P_k(\alpha, \alpha)$ denotes an average over the nodes of the network.

IV. HOMOGENEOUS PHASES AND COUPLED DYNAMICS ON NETWORK

A. Homogeneous phase and network properties

We shall now connect the *symbolic homogeneity* with network properties. When all the nodes in a network have the same degree and the network is homogeneously connected, i.e. if the network is completely symmetric, like a nearest neighbour coupled network with periodic boundary conditions, then, unless the dynamics breaks the symmetry, each node should have *qualitatively the same symbolic dynamics*, i.e. all transition probabilities for all the nodes being equal. In fact, one might then even expect stability of the synchronized state, but that in general is not true for all coupling strengths. Homogeneous symbolic dynamics need not correspond to synchronization, though it may correspond to phase synchronization. For random networks, homogeneity of the symbolic dynamics depends on the number of connections in the network. Note that depending upon the coupling strengths, for certain network architecture one may get all the three phases, including the homogeneous synchronized phase. Using the master stability function which takes local dynamics as well as network architecture into account, one can deduce the coupling strength region for which the coupled dynamics would be synchronized [18]. To relate different dynamical

states with the network parameters, we consider the quantity $r = \frac{N_c}{N(N-1)/2} \sim N_c/N^2$. This ratio compares the number of connections N_c in the network with the number of possible connections $N(N-1)/2$. We use r as an indicator to roughly distinguish the three phases. For r being close to one (number of connections N_c of order N^2), we get a fully synchronized state for appropriate coupling strengths ε . Then the transition probabilities of all nodes are obviously equal (phase 3). For $N_c \sim N$, we get phase two, i.e. the nodes are partially synchronized or partially phase synchronized, but the symbolic dynamics of the nodes are identical. Note here we are only roughly relating N_c and phase, later we will provide a more accurate relation between the number of connections and the phases.

B. Symbolic synchronized phase and global properties of coupled dynamics

We concentrate on the phase where the nodes are not synchronized though their symbolic dynamics are identical. This is the most interesting phase as the complexity of the coupled dynamics can be understood by observing the symbol sequence of any arbitrarily selected node. Fig. 1 is plotted for the logistic map as the local map and a scale-free network [23] as the coupling network. Figs. (a),(b),(c) and (d) plot the variation of synchronization measure (σ^2), and measure of homogeneity (ς^2) as a function of coupling strengths and Fig. (a'), (b'), (c') and (d') plot the transition probability $P(\alpha, \alpha)$ for different nodes. We start with the example of networks having coupled dynamics in phase one (non-homogeneous unsynchronized) and we move towards the examples of networks showing homogeneous synchronized state, phase 3.

For $\varepsilon < 0.2$, the coupled logistic map model (4) exhibits a similar behaviour for different coupling architectures, with quasiperiodic behaviour around $\varepsilon = 0.2$. The behaviour varies with the coupling architecture for larger coupling strengths. In the periodic regions the symbolic dynamics of the nodes, given by (3), would always be similar irrespective of the underlying coupling network. So, in the periodic regions we do not get any extra information about the network by observing symbolic sequences, but the symbolic dynamics is informative when the coupled dynamics lies on the chaotic attractor. Subfigures 1(a), (a'), are plotted for scale free networks with average degree 2. The transition probabilities $P(\alpha, \alpha)$ are completely different for the different nodes (except for $\varepsilon < 0.2$). Here, the nodes are not synchronized, σ^2 being nonzero for the entire coupling strength range.

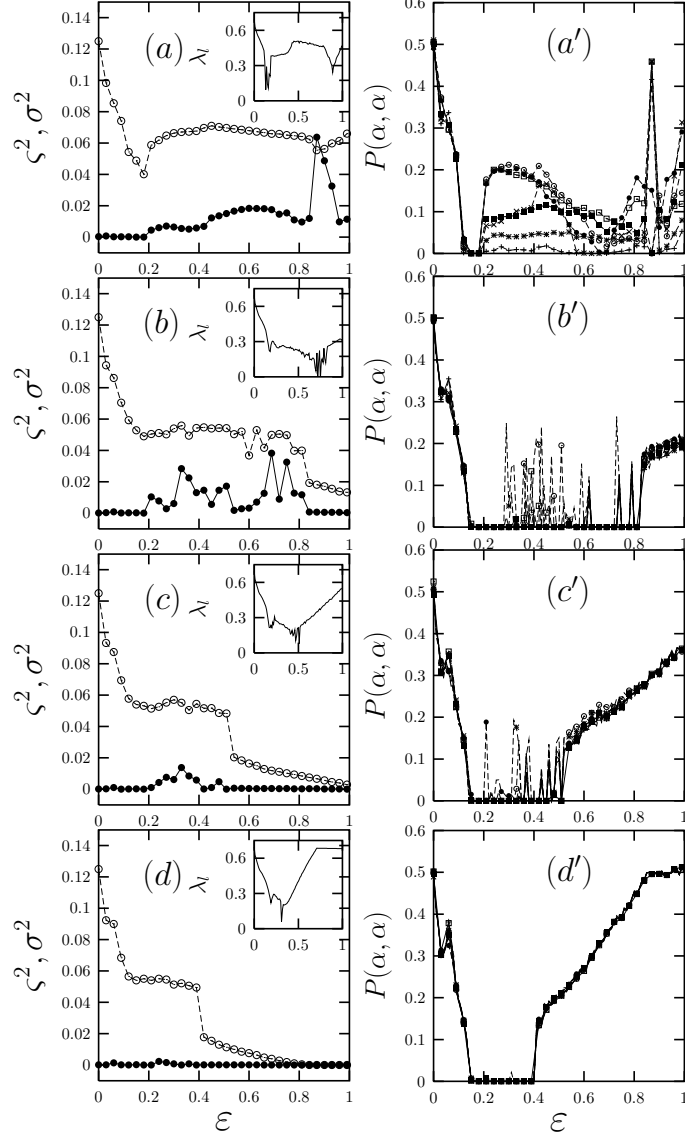


FIG. 1: Examples of coupled networks showing all three phases. All figures are plotted for scale-free networks, generated by using BA algorithm [19], of size $N = 200$ and (a) average degree 2 (phase 1), (b) average degree 6, (c) average degree 10, (d) average degree 20. The x -axis represents the coupling strength and the y -axis gives the synchronization measure σ^2 (\circ) and the homogeneity measure ζ^2 (\bullet) for the whole network. The largest Lyapunov exponent is plotted as a function of the coupling strength (see inset). Figs. (a'), (b'), (c') and (d') show exact values of the transition probability $P(\alpha, \alpha)$ for different nodes as a function of the coupling strength. For clarity we plot only a few arbitrarily selected nodes.

This state corresponds to *phase one*. Interesting phenomena occur when we increase the number of connections in the networks. Subfigures 1(b) and (b') are plotted for a scale-free network with average degree 6. It can be seen that $P(\alpha, \alpha)$ for different nodes are remarkably similar. Note that we calculate $P(\alpha, \alpha)$ for coupled dynamics being in the chaotic and unsynchronized regime (λ_l and σ^2 both are greater than zero). So we do not take periodic and synchronized regions into account which obviously yield similar symbolic dynamics for all the nodes. This homogeneity becomes more prominent as we increase the number of connections in the network. In Figs. 1(c), (c') and 1 (d), (d'), The transition probabilities of all the nodes are the same except for a few places where some nodes have different transition probability (e.g. node number 50 in (c') having a different value of $P(\alpha, \alpha)$). Note that here the nodes are not synchronized, which is indicated by the nonzero value of σ^2 throughout the coupling range, except for $\varepsilon = 1$ in (c) and for $\varepsilon > 0.8$ in (d).

The second interesting feature is the qualitatively similar behaviour of the largest Lyapunov exponent, which is calculated from (4), and $P(\alpha, \alpha)$, which is calculated from a scalar time series of an arbitrarily selected node. Note that the time series used for the calculation of $P(\alpha, \alpha)$ is very short compared to the traditional methods to calculate the largest Lyapunov exponent from a scalar time series. This similar behaviour of the Lyapunov exponent and the ordering relations between the values of the state variable was first observed by Bandt and Pompe [10] in the case of isolated dynamics. Here we show that a similar relation exists for coupled dynamics, depending upon the network parameters, namely the connection architecture and the connection ratio N_c/N^2 .

Fig. 2 is plotted for various networks being in the *phase two* (homogeneous unsynchronized phase). They show the similar behaviour of λ_l and $P(\alpha, \alpha)$ of any arbitrarily selected node. For k -nearest neighbour coupled networks we always find the homogeneous phase, independent of the average degree or the ratio N_c/N^2 . This is because of the symmetry between the nodes. In all the subfigures, $P(\alpha, \alpha)$ qualitatively matches with the largest Lyapunov exponent of the coupled dynamics. At certain ε values $P(\alpha, \alpha)$ is almost zero, whereas λ_l is positive. This indicates ordered behaviour (Ref. [14]) of the coupled system, for example Fig.2(c) and Fig.4(c) are plotted for the same network. When $P(\alpha, \alpha)$ is very small the coupled dynamics is in the high state of the phase synchronization (Fig.4(c)) (i.e. almost all nodes are forming phase synchronized cluster(s) Ref.[14]) though the largest Lyapunov exponent still remains positive (Fig.2(c)).

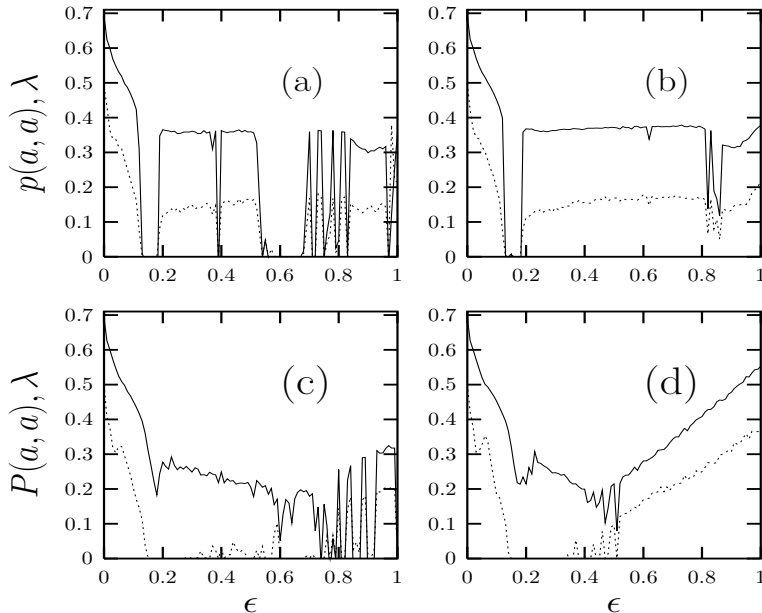


FIG. 2: The global measure of coupled dynamics from the local symbolic dynamics. We take various networks having coupled dynamics in the *phase two*. The x -axis gives the coupling strength ϵ and the y -axis depicts λ_l (-)(largest Lyapunov exponent for the coupled dynamics) as well as $P(\alpha, \alpha)$ (...)(transition probability for a randomly selected node). (a) for nearest neighbour coupled network of size $N = 20$, (b) for 3-nearest neighbour coupled network, $N = 50$, (c) and (d) are for random and scale-free networks, respectively, with average degree 10 and $N = 200$.

In *phase three*, which is synchronized phase, the largest Lyapunov exponent would simply be the Lyapunov exponent of the uncoupled map and all the nodes will have the same transition probability as of the uncoupled node.

V. RELATION BETWEEN DYNAMICAL PHASES AND NETWORK PROPERTIES

We can also exhibit a direct relation between network parameters and dynamical behaviour. The symmetry properties of the network and the connection density affect the homogeneity of the symbolic sequences. Fig. 3 plots the deviation from the homogeneity indicated by $\varsigma_\epsilon^2 = \left\langle \frac{1}{N} \sum_{i=1}^N [P_i(\alpha, \alpha) - \overline{P(\alpha, \alpha)}] ^2 \right\rangle_\epsilon$, as a function of $2N_c/N(N-1)$. Here, P_i is the transition probability of i th node and $\overline{P(\alpha, \alpha)} = \frac{1}{N} \sum_{i=1}^N P_i(\alpha, \alpha)$, and $\langle \cdot \rangle_\epsilon$ denotes the average over all coupling strengths. We start with one-dimensional nearest neighbour cou-

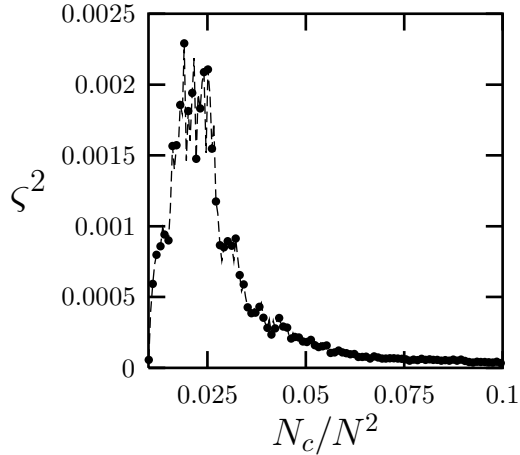


FIG. 3: The measure of homogeneity ζ^2 as a function of the connectivity ratio $2N_c/N(N-1)$.

pled network (homogeneous phase) and randomly add connections. For nearest neighbour coupled networks we obtain the homogeneous phase, as already explained in the previous section. As we add the connections randomly, first the homogeneity gets perturbed, but gets reestablished as the number of connections is increased further. Note that here we always calculate the deviation in the non-synchronized regime only, because the synchronized regime obviously corresponds to the homogeneous phase. For each randomly added connection we take the average of the twenty networks. Note that in this region (phase two) σ^2 is not zero. For N_c/N^2 close to one, we get a synchronized state after a coupling strength [21] that corresponds to the homogeneous state (phase three). Note that for the local dynamics in the chaotic regime, only the network property seem to be responsible for the homogeneous or non-homogeneous behaviour of the coupled dynamics. Fig. 3 is plotted for the coupled logistic map but a similar behaviour is shown by the Hénon maps also (see section VII).

VI. PHASE SYNCHRONIZATION : SYMBOLIC SYNCHRONIZATION

If nodes i and j have the same symbolic dynamics, $s_t(i) = s_t(j)$, then we say nodes i, j are symbolically synchronized. Also, a cluster of nodes is symbolically synchronized if all pairs of nodes belonging to that cluster are symbolically synchronized. Note that in a symbolically synchronised cluster, the state values of the nodes may differ. The symbolic synchronization is observed in the *phase two*, where the number of the connections in the networks is very small, in general of the order of N . With the increase in the number of connections we

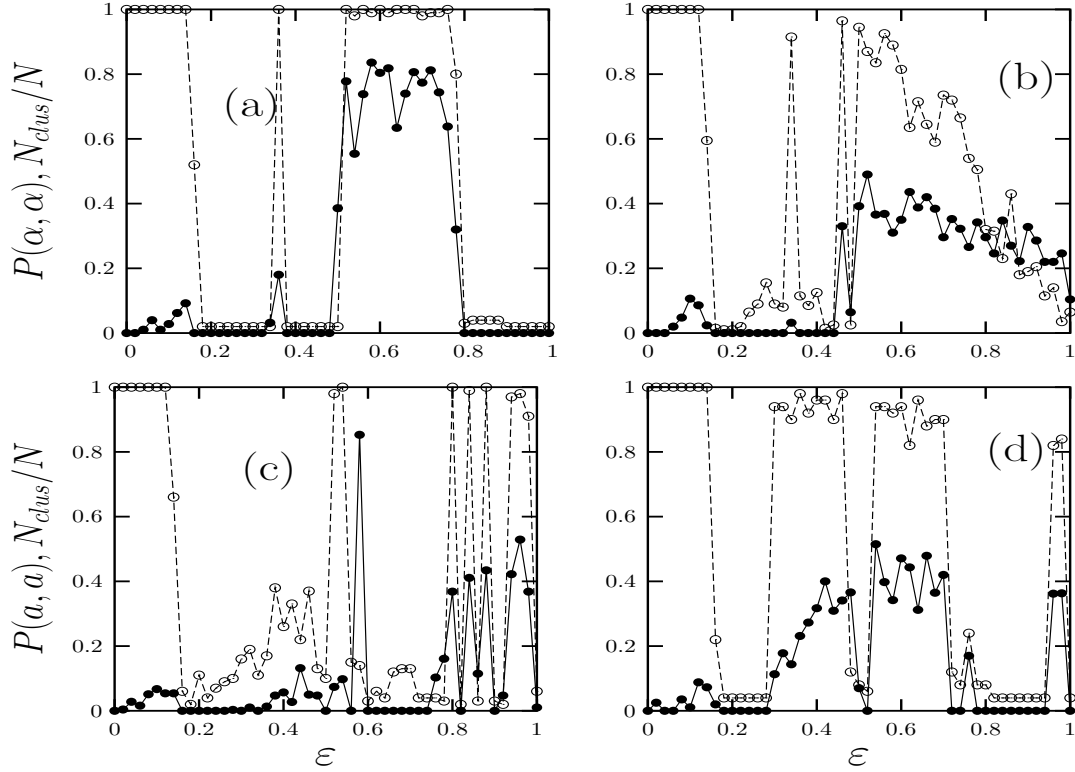


FIG. 4: The ratio of the number phase synchronized clusters to the maximum possible clusters, N_{clus}/N and the transition probability $P(\beta, \beta)$ for the coupled logistic map as a function of the coupling strength ε , (a) for a nearest neighbour coupled network with average degree 20 and $N = 100$, (b) for a scale-free network with average degree 10 and $N = 100$, (c) for a random network with average degree 10 and $N = 100$, (d) for a nearest neighbour coupled network with average degree 6 and $N = 50$, and the tent map ($f(x) = (1 - 2|x - \frac{1}{2}|)$) as the local chaotic function.

usually get a fully synchronized cluster, which is trivially symbolically synchronized. Many real-world networks are sparsely connected ($N_c \ll N$), and complete synchronization is relatively rare, though phase synchronization or symbolic synchronization is possible. We show that $P(\beta, \beta)$ can be used as a good measure of the phase synchronization in the coupled map network (4). Fig. 4 shows the correlation between the phase synchronization and the transition probability $P(\beta, \beta)$ of an arbitrary selected node. We see that in the homogeneous region $P(\beta, \beta)$ matches considerably well with the phase synchronization. Note that in partially ordered phase region, phase synchronized clusters vary with time. We plot the number of clusters calculated for a certain time length, and the number of clusters may change with the evolution of the coupled dynamics. Therefore at some coupling strength

region(s), the transition probability $P(\beta, \beta)$ does not match with the phase synchronization (For example in the Fig. 4(c), at coupling strength 0.59, the value of $P(\beta, \beta)$ is very high although the nodes are phase synchronized).

VII. COUPLED HÉNON MAPS

In this section we apply our method to coupled Hénon maps. The Hénon map is a two-dimensional map [22],

$$\begin{aligned}x(t+1) &= y(t) + 1 - ax(t)^2 \\ y(t+1) &= by(t).\end{aligned}$$

When one introduces the possibility of a time delay, the above equation can be written as the scalar equation,

$$x(t+1) = bx(t-1) + 1 - ax(t)^2 \quad (6)$$

For the parameters we take the values $a = 1.4$ and $b = 0.3$, for which the Hénon map is known to have a chaotic attractor.

We define the symbolic dynamics as given in (3). The choice of the threshold x^* requires some care. A judicious choice should make certain short transition probabilities very small, which may be useful for detecting network dynamics from single-node measurements [8]. Clearly, increasing the threshold decreases the probability of occurrence of the repeated sequence $\beta\beta$. However, it also decreases the probability of observing the single symbol β , making it difficult to work with short time series. Hence, the choice of the threshold is a compromise between these two effects. We use the natural density defined by the data to choose a threshold. Fig. 5 depicts how the the probabilities of observing a single symbol β and the repeated sequence $\beta\beta$ change depending on the value of the threshold x^* . It can be seen that a choice of x^* roughly in the range $(0.55, 1.20)$ would be useful, since it renders the sequence $\beta\beta$ very unlikely without constraining the occurrence of the symbol β . Note that it is immediate from their definitions that the probabilities $P(\beta)$ and $P(\beta, \beta)$ will be decreasing as functions of x^* , and will approach zero as x^* increases; furthermore, $P(\beta) > P(\beta, \beta)$. It follows that one can find a threshold x^* for which $P(\beta)$ is large compared to $P(\beta, \beta)$. Fig. 5 shows the ratio $P(\beta, \beta)/P(\beta)$, and the sharp decrease at about $x^* \approx 0.6$ suggests to take some value near 0.6 as the threshold, yielding a very small $P(\beta, \beta)$ and a large $P(\beta)$ at the

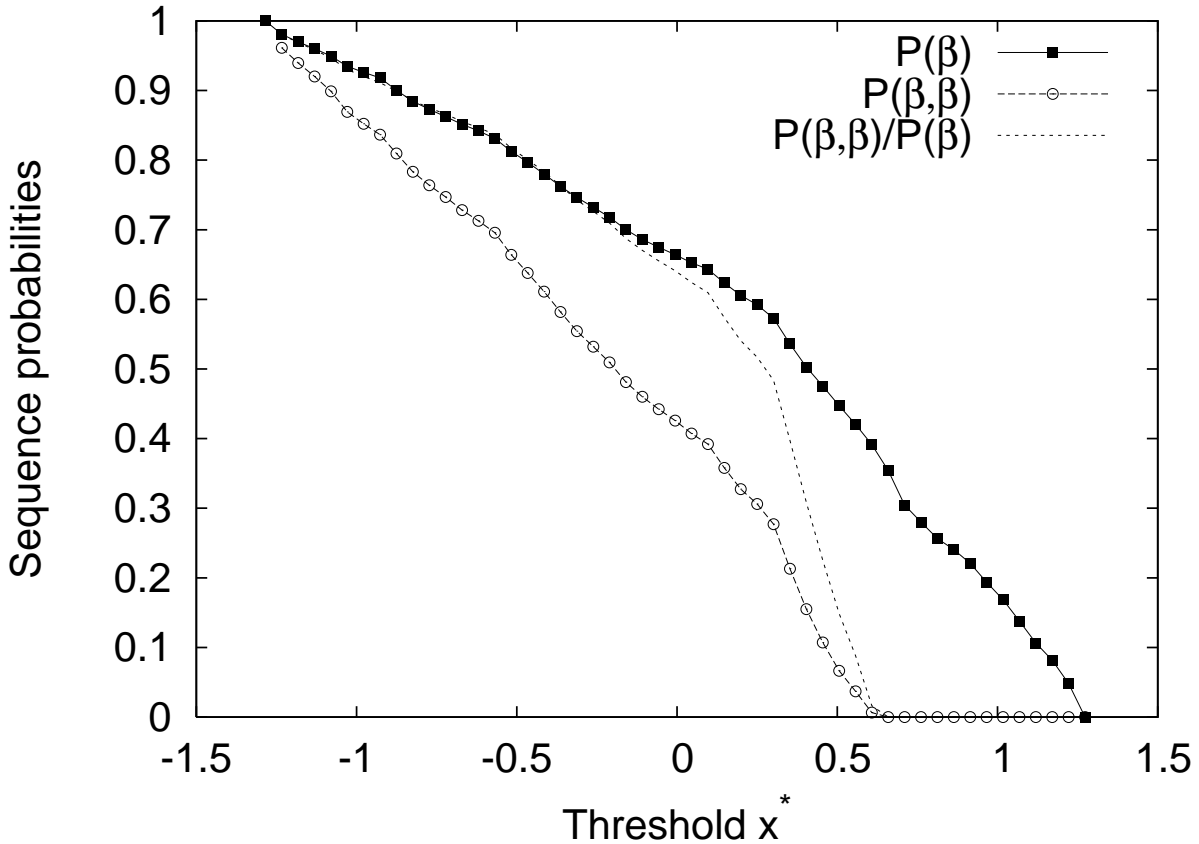


FIG. 5: Illustration of the choice of the threshold x^* as the point where $P(\beta, \beta)/P(\beta)$ sharply drops to near zero.

same time. We evolve (4) starting from random initial conditions, with (6) as local dynamics, and estimate the transition probabilities $P(i, j)$ as discussed in the first section, using a time series of length $\tau = 1000$. At the globally synchronized state $x_i(t) = x_j(t); \forall i, j, t$, with all nodes evolving according to the rule (6), the symbolic sequences measured from a node will be subject to the same constraints as that generated by (6).

We now discuss some results based on numerical simulations on various networks. Fig. 6 plots the transition probabilities as a function of the coupling strength. We consider the symbolic sequences of length two and three. For length two, we consider the transition probabilities $P(\alpha, \alpha)$ and $P(\beta, \beta)$. For sequences of length three we have 6 possible transitions, but some of them are very small (like $P(\beta, \beta, i)$, i being α, β), so we plot only those transition probabilities which vary with the couplings. It is clear from the figures that the synchronized state is easily detected by looking at the transition probabilities of any

arbitrarily selected node. Whenever the transition probabilities are equal to the transition probabilities of the map (6), the network is globally synchronized. It is clear from subfigures (d),(e) and (f) that for the synchronized region (zero σ^2), the deviation of transition probabilities from the transition probabilities of the uncoupled map (6) is also zero. Here, the deviation of $P(i, j)$ of any node is defined as $\delta_{i,j}^2 = \left\langle \frac{1}{m-1} \sum_{k=1}^m [P_k(i, j) - \overline{P(i, j)}]^2 \right\rangle$, where $\overline{P(i, j)} = \frac{1}{m} \sum_k P_k(i, j)$, calculated at $\varepsilon = 0$ $k = 1, \dots, m$ are m different sets of random initial conditions taken between -1.5 and 1.5 . In all the figures (except (f)) we get synchronization for larger coupling strengths, so the deviation is almost zero there, i.e. all transition probabilities match completely with those of the uncoupled map. Note that there are certain regions (small coupling strength range $\varepsilon < 0.2$) where the nodes do not get synchronized while the deviations are quite small. That is because for sufficiently small coupling strength, couplings do not affect the behaviour of the individual nodes very much, and so the transition probabilities do not differ much from those corresponding to the uncoupled function. However, as we increase the coupling strength, the transition probabilities become dependent on the couplings. Still, if we look at the small coupling strength regions carefully we see that not all the deviations are small. For example, although the deviations of $P(\beta, \alpha, \alpha)$ (- - -) and $P(\alpha, \alpha, \beta)$ (-) are very small, the deviation in $P(\alpha, \alpha, \alpha)$ (...) is still large, whereas for the synchronized regime all deviations are very close to zero. Fig. 7 plots the deviation from the homogeneity ζ^2 as a function of N_c/N^2 (see the caption of Fig. 3, which shows a similar plot with logistic map as a local dynamical function). The only difference is that for the Hénon map we plot the transition probability of three-symbol sequences instead of two-symbol sequences for logistic and tent maps.

VIII. CONCLUSION

We have studied the symbolic dynamics of coupled maps on networks. We define our symbolic dynamics based on non-generating partitions leading to some forbidden transitions of symbols in the time evolution of the function. The optimal partitions are those which lead to the maximal difference between the permutation entropy of the dynamical iteration and corresponding random iteration. For one-dimensional systems finding these partitions is simple, whereas for higher dimensional systems it may be more difficult. However, it turns out that symbolic dynamics drawn from any non-generating partitions is usually good

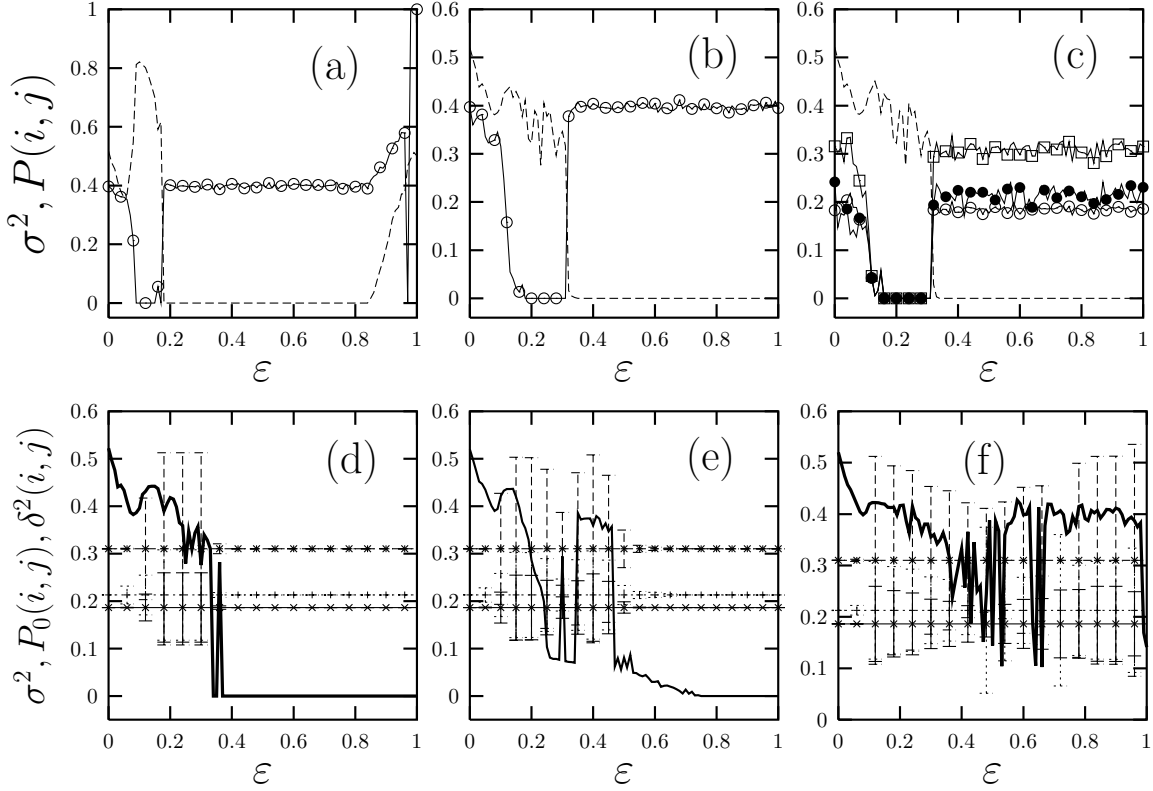


FIG. 6: The transition probability measure for coupled Hénon maps. The x -axis displays the coupling strength and the y -axis shows the different transition probabilities and the measure of synchronization σ^2 . (a) is for two coupled nodes and plots $P(\alpha, \alpha)$ for the symbolic sequence of length 2. (b) and (c) are plotted for globally coupled networks with $N = 50$. (b) plots $P(\alpha, \alpha)$ and (c) plots transition probabilities for symbolic sequences of length 3, namely $P(\alpha, \alpha, \alpha)$ (\square), $P(\alpha, \alpha, \beta)$ (\bullet), and $P(\beta, \alpha, \alpha)$ (\circ). The synchronized state is detected when all the transition probabilities are equal to those of the uncoupled map; i.e. the transition probabilities at the zero coupling strength. (d), (e) and (f) show the standard deviation σ^2 (solid thick line) and δ^2 (vertical dashed line) for these three transition probabilities of an arbitrary selected node with respect to the transition probabilities of the uncoupled function (solid line), i.e for $\varepsilon = 0$. δ^2 is calculated for 20 simulations for the dynamics with different sets of random initial conditions. (d) for a globally connected network with $N = 50$, (e) and (f) for a random network with $N = 100$, average degree 10 and 2 respectively. The last subfigure is plotted to show the behaviour of the transition probabilities when we do not get global synchrony even at large coupling strengths.

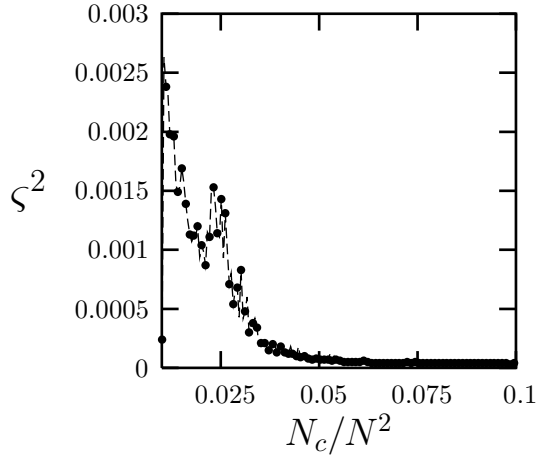


FIG. 7: The measure of homogeneity ζ^2 as a function of connection ratio $2N_c/N(N-1)$, with Hénon map as the local dynamical function.

enough for the applications we have considered in this paper. The symbolic dynamics can be drawn when the system parameters are not known, as well as for experimental data taken in a noisy environment.

We use symbolic dynamics as a measure of dynamical state of the coupled system and show various applications of this measure. We define three different states of the coupled dynamics based on the synchronization and the symbolic dynamical properties. In the homogeneous synchronized phase, complete synchrony is detected by comparing the transition probabilities of any arbitrarily selected node with those of the uncoupled function. In this state the coupled dynamics collapses to the dynamics of the uncoupled function, and the symbolic dynamics of any node is subject to the same constraints as that generated by the uncoupled function.

Phase two, which refers to the *homogeneous unsynchronized phase* or *symbolic synchronized phase*, is of our prime interest where the nodes are not synchronized but have identical symbolic dynamics. Although these phases are detected dynamically, we find that the homogeneous unsynchronized phase is related to the connection density (N_c/N^2) and to a smaller extent to the chaotic dynamical function used. This region is generally observed for networks with $N_c \sim r \times N^2$ where $0.05 < r < 0.1$. Most of the real networks are sparsely connected and come under the category of phase two. In this phase we can deduce the global properties of the coupled dynamics such as the largest Lyapunov exponent and phase synchronization by simply observing the local symbolic dynamics of any randomly selected

node.

As it is expected from such a simplistic reduction, our symbolic dynamics gives only the qualitative understanding. A more precise calculation of complexity through some entropy measure of the system based on the symbolic dynamics is one of the future steps. Further future investigations will involve an analytical understanding of symbolic synchronization and application to detect various levels of synchronization in experimental data taken from coupled systems.

-
- [1] K. Kaneko, *Formation, Dynamics and Statistics of Pattern*, Edited by K. Kawasaki et al. (World Sci., Singapore, 1990).
 - [2] K. Kaneko, *Chaos* **2**, 279 (1992).
 - [3] S. Jalan and R. E. Amritkar, *Indian Natn Sci Acad* **71** , **A** No. 1-2 (2005).
 - [4] D. Lind and B. Marcus, *An introduction to Symbolic Dynamics and Coding* (Cambridge Univ. Press, 1995).
 - [5] Bai-Lin Hao and Wei-Mou Zheng, *Applied Symbolic Dynamics and Chaos* (Word Sci., Singapore, 1998).
 - [6] A. Endler and J. A. C. Gallas, *Phys. Rev. E* **65**, 036231 (2002); R. L. Davidchack, Y.-C. Lai, E. M. Boltt, and M. Dhamala, *Phys. Rev. E* **61**, 1353 (2000); A. Witt, R. Braun, F. Feudel, C. Grebogi, and J. Kurths, *Phys. Rev. E* **59**, 1605 (1999); E. Boltt and Y.-C. Lai, *Phys. Rev. E* **58**, 1724 (1998); W.-M. Zheng, *Phys. Rev. E* **56**, 1556 (1997); F. Christiansen and A. Politi, *Phys. Rev. E* **51**, R3811 (1995).
 - [7] Leonid A. Bunimovich, *Physica D* **103**, 1 (1997); S. D. Pethel, N. J. Corron and E. Boltt, *Phys. Rev. Lett.* **96**, 034105 (2006).
 - [8] S. Jalan, F. M. Atay, and J. Jost (nlin.CD/0510057).
 - [9] H. Voss and J. Kurths, *Phys. Rev. E* **58**, 1155-1158 (1998).
 - [10] C. Bandt and B. Pompe, *Phy. Rev. Lett.*, **88** 174102 (2002).
 - [11] A. Pikovsky, M. Rosenblum and J. Kurths, *Synchronization : A Universal Concept in Non-linear Dynamics* (Cambridge Univ. Press, 2001).
 - [12] S. Boccaletti, J. Kurths, G. Osipov, D.L. Valladares and C. S. Zhou, ‘The Synchronization of Chaotic Systems, *Phys. Rep.* **366**, 1 (2002).

- [13] T. Zhou, L. Chen and K. Aihara, *Phys. Rev. Lett.* **95**, 178103 (2005); R. E. Amritkar, S. Jalan and C. K. Hu, *Phys. Rev. E* **72**, 016212 (2005); I. Belykh, E. de Lange, and M. Hasler, *Phys. Rev. Lett.* **94**, 188101 (2005); D.-U. Hwang, M. Chavez, A. Amann, and S. Boccaletti, *Phys. Rev. Lett.* **94**, 138701 (2005); A. Zumdieck, M. Timme, T. Geisel, and F. Wolf, *Phys. Rev. Lett.* **93**, 244103 (2004); M. G. Rosenblum and A. S. Pikovsky, *Phys. Rev. Lett.* **92**, 114102 (2004); H. Xiao, G. Hu, and Z. Qu, *Phys. Rev. Lett.* **77**, 4162-4165 (1996); . Corral, C. J. Prez, A. D-Guilera, and A. Arenas, *Phys. Rev. Lett.* **74**, 118-121 (1995).
- [14] M. G. Rosenblum, A. S. Pikovsky, and J. Kurths, *Phys. Rev. Lett.* **76**, 1804 (1996); S. Jalan and R. E. Amritkar, *Phys. Rev. Lett.*, **90** 014101 (2003); S. Jalan, R. E. Amritkar, C. K. Hu, *Phys. Rev. E*, **72**, 016211 (2005).
- [15] J. Jost and K. M. Kolwankar, *Fractals in Engineering - New Trends in Theory and Applications*, page 57 (Springer, London, 2005).
- [16] H. D. I. Abarbanel, R. Brown, J. J. Sidorowich, and L. Sh. Tsimring, *Rev. Mod. Phys.* **65**, 1331-1392 (1993).
- [17] K. Kaneko, *Physica D* **34**, 1-41 (1989).
- [18] L. M. Pecora and T. L. Carroll, *Phys. Rev. Lett.* **80**, 2109 (1998).
- [19] A. -L. Barabasi, R. Albert, H. Jeong, *Physica A*, **281**, 69 (2000).
- [20] F. M. Atay, T. Biyikoglu, and J. Jost, *IEEE Trans. Circuits and Sys. I*, **53(1)**, 92-98, 2006.
- [21] R. E. Amritkar, S. Jalan and C. K. Hu, *Phys. Rev. E* **72**, 016212 (2005).
- [22] A. J. Lichtenberg and M. A. Lieberman, *Regular and Chaotic Dynamics* (Springer-Verlag, 1983).
- [23] We have generated that scale-free network by the standard preferential attachment scheme [19], but one should note that large classes of scale-free networks may exhibit a qualitatively different behaviour as regards other crucial network parameters besides the degree sequence, in particular concerning synchronizability, see [20].